Migrating and nonmigrating diurnal tides in the middle and upper atmosphere excited by tropospheric latent heat release

M. E. Hagan
National Center for Atmospheric Research, Boulder, Colorado, USA

J. M. Forbes
University of Colorado, Boulder, Colorado, USA

Received 17 August 2001; revised 15 December 2001; accepted 18 December 2001; published 19 December 2002.

[1] The global-scale wave model (GSWM) is used to investigate mesospheric and lower thermospheric migrating and nonmigrating diurnal tidal components that propagate upward from the troposphere, where they are excited by latent heat release associated with deep tropical convection. Our diurnal tidal forcing parameterization is derived from a 7-year database of global cloud imagery. The GSWM migrating response is sufficiently large to modulate the dominant radiatively excited migrating diurnal tide in the middle and upper atmosphere during every month of the year. Five additional nonmigrating diurnal components, the eastward propagating zonal wave numbers 2 and 3, the westward propagating zonal wave number 2, and the standing oscillations, also introduce significant longitudinal variability of the diurnal tide in these regions. The comparative importance of the nonmigrating components evolves from month to month and varies with tidal field. Our GSWM investigation suggests that other dynamical models must account for the tropospheric latent heat source in order to make realistic predictions of the diurnal tide in the middle and upper atmosphere. *INDEX TERMS:* 3384 Meteorology and Atmospheric Dynamics: Waves and tides; 3367 Meteorology and Atmospheric Dynamics: Theoretical modeling; 3369 Meteorology and Atmospheric Dynamics: Thermospheric dynamics (0358); 3332 Meteorology and Atmospheric Dynamics: Mesospheric dynamics; *KEYWORDS:* atmospheric tides, migrating tides, nonmigrating tides, dynamical coupling

Citation: Hagan, M. E., and J. M. Forbes, Migrating and nonmigrating diurnal tides in the middle and upper atmosphere excited by tropospheric latent heat release, *J. Geophys. Res.*, *107*(D24), 4754, doi:10.1029/2001JD001236, 2002.

1. Introduction

[2] Atmospheric solar tides are global-scale waves with periods that are harmonics of a solar day. They can be excited by the absorption of solar radiation, by large-scale latent heat release associated with deep convective activity in the troposphere, by nonlinear interactions between global-scale waves [e.g., *Miyahara and Miyoshi*, 1997; *Hagan and Roble*, 2001; *McLandress*, 2001], by interaction between gravity waves and tides [e.g., *McLandress and Ward*, 1994], and to a lesser extent by the gravitational pull of the Sun. Migrating tidal components propagate with the apparent motion of the sun. Thus, the migrating diurnal tide is a westward propagating $s = -1$ perturbation with a period of 24 hours, where the magnitude of s represents the zonal wave number and the sign of s represents the direction of propagation (positive eastward). So-called nonmigrating solar diurnal tidal components are $s \neq -1$ global perturbations with periods of 24 hours. These waves can be standing (i.e., $s = 0$), or they can propagate eastward (i.e., $s > 0$) or westward (i.e., $s < 0$). Since their zonal wave numbers are not equal to the frequency (day^{-1}) of the wave, nonmigrating tides have different longitudinal characteristics than their migrating counterparts. Recent analyses of Upper Atmosphere Research Satellite (UARS) measurements [*Khattatov et al.*, 1996; *Hagan et al.*, 1997b] reveal longitudinal diurnal tidal variability which the authors attributed to the presence of nonmigrating components. In a comprehensive study of both UARS winds and temperatures, *Talaat and Lieberman* [1999] quantified the altitudinal and monthly evolution of the $s = 0$, $s = 1$, $s = 2$, and $s = 3$ diurnal tidal components in these data. In this report we describe a numerical investigation of one plausible source of nonmigrating diurnal tides in the MLT.

[3] Subsequent to the seminal work of *Chapman and Lindzen* [1970] on classical tidal theory, researchers invoked increasingly realistic models to numerically investigate the effects of tidal excitation, propagation, and dissipation in the atmosphere. The extensive body of achievements is discussed in a series of review papers and tutorials [*Forbes and Garrett*, 1979; *Kato*, 1980; *Forbes*, 1984, 1995; *Volland*, 1988; *Vial*, 1989; *Vial and Forbes*, 1989; *Hagan*, 2000]. The dominant migrating tidal components that are thermally driven by the periodic absorption of solar radiation throughout the atmosphere are the foci of most of the tidal modeling

0148-0227/02/2001JD001236

efforts to date. But, nonmigrating tides are also investigated in this body of work, and they emerge as important sources of tidal variability. The first attempts to model nonmigrating tides assumed that their source was the nonuniform global distribution of solar irradiance absorption in the atmosphere [e.g., *Kato et al.*, 1982]. Investigators used both linearized [*Forbes and Groves*, 1987; *Tsuda and Kato*, 1989], and general circulation models (GCM) [*Tokioka and Yagai*, 1987; *Yagai*, 1989] to explore the effects of these waves as they propagated away from their source. Follow-on attempts to model nonmigrating tides continued to focus on the lower and middle atmosphere [e.g., *Lieberman and Leovy*, 1995], until *Williams and Avery* [1996] extended the calculations of *Forbes and Groves* [1987] and used a 1-dimensional windless and inviscid linear tidal model to explore nonmigrating diurnal tidal signatures in the mesosphere and lower thermosphere (MLT). *Williams and Avery* [1996] also used this simple model to investigate the tidal responses to tropospheric latent heat sources inferred from a 1-year global cloud imagery (GCI) database. Their results suggested that nonmigrating tides may significantly modulate the migrating tide in the MLT.

[4] *Lindzen* [1978] and *Hong and Wang* [1980] independently proposed that latent heat release associated with cloud and/or raindrop formation could be a significant tidal source. Using rainfall data in combination with numerical experiments, *Hamilton* [1981] critically examined latent heat release as a possible tidal excitation mechanism and provided strong support for the theory. In particular, he concluded that its diurnal variation should be significant and noted that diurnal surface pressure variations are characterized by large geographic variations which cannot be explained by the migrating tide [*Hamilton*, 1981].

[5] *Hagan et al.* [1997a] employed the *Williams and Avery* [1996] heating rates in the global-scale wave model (GSWM) to produce comparatively more realistic migrating and nonmigrating tidal responses between the ground and the lower thermosphere. They reported that tropospheric nonmigrating radiative forcing did not contribute to MLT diurnal tidal dynamics. However, nonmigrating diurnal tides excited by latent heat release introduced measurable ($\sim$10 m/s) longitudinal variability in their MLT solutions, even though they were individually up to 3 times smaller than their migrating diurnal tide. Using a linear tidal model that is similar to GSWM, *Ekanayake et al.* [1997] showed that upward propagating nonmigrating diurnal tides posses significant amplitudes at MLT low and middle latitudes. When they forced their model with the combined Kyushu University GCM (KU-GCM) radiative and dry and latent convective heat sources [*Miyahara et al.*, 1993], they found that eastward propagating components dominated all but the migrating diurnal response during southern hemisphere summer. *McLandress* [1997] also investigated the effects of both solar radiative and deep convective tidal sources, and quantified the seasonal variability of the diurnal tide in the MLT using heating rates from the Canadian Middle Atmosphere Model (CMAM).

[6] *Forbes et al.* [1997] analyzed 7 years of GCI data in order to quantify annually averaged migrating tidal heating rates due to latent heat release. They forced GSWM with these heating rates and reported MLT migrating diurnal and semidiurnal temperature and wind responses of 5–10°K and 10–20 m/s, respectively. These authors also conducted a correlative analysis of rain gauge data to confirm that GCI is a viable proxy for rainfall rate. The paucity of oceanic rain gauge data motivated the use of satellite-borne diagnostics for this and other global studies [e.g., *Williams and Avery*, 1996]. The strong correlation between these data validates the efforts to infer large-scale tropospheric latent heating rates from the satellite diagnostics.

[7] Because their correlative rain gauge data were annually averaged, *Forbes et al.* [1997] exclusively investigated the associated annually-averaged tidal perturbations. However, the GCI data set that they analyzed is sufficiently robust that we can use it to deduce monthly-averaged migrating and nonmigrating diurnal and semidiurnal heating rates. We report herein on the diurnal subset of the tidal solutions that we obtained when we forced GSWM with such monthly rates. In the following section, we describe the GSWM and our parameterization of tidal forcing due to latent heat release [after *Forbes et al.*, 1997; *Williams and Avery*, 1996]. Subsequently, we highlight the results that we obtained with GSWM for 12 months of the year. We discuss representative solutions, the April and August diurnal perturbations, in some detail. We conclude with an assessment of the importance of the tropospheric latent heat source to MLT diurnal tidal dynamics and the implications of our findings for future observational and numerical studies of atmospheric tides.

2. GSWM

2.1. Model Overview

[8] The GSWM is a 2-dimensional, linearized, steady-state numerical tidal and planetary wave model which extends from the ground to the thermosphere [*Hagan et al.*, 1993, 1995, 1999] (see also information available from the High Altitude Observatory at http://www.hao.ucar.edu/public/research/tiso/gswm/gswm.html). Briefly, GSWM tidal and planetary wave predictions are solutions to the linearized and extended Navier-Stokes equations for perturbation fields with characteristic zonal wave numbers and periodicities that are assumed a priori along with the zonal mean background atmosphere. Mean zonal (meridional) winds are included (neglected). The most recent version of the model, hereafter GSWM-00 [e.g., *Hagan et al.*, 2001], produced monthly migrating tidal climatologies and is a simple extension to GSWM-98 [*Hagan et al.*, 1999]. Briefly, the seasonally variable GSWM-98 tropospheric heating rates [*Hagan*, 1996] and effective Rayleigh friction coefficients [*Hagan et al.*, 1999] were linearly interpolated for the GSWM-00 calculations. The remaining inputs and forcings vary with month inherently and remain consistent with those invoked for GSWM-98. We implemented the GSWM-00 inputs and parameterization schemes in the calculations that we report herein with the exception of the radiative tidal forcing functions. Those were replaced with the parameterization that is described in the following section. We overview the GSWM background atmosphere and dissipative schemes in the paragraphs below.

[9] From the ground into the upper thermosphere GSWM background temperatures and densities are specified by MSISE90 [*Hedin*, 1991]. Below $\sim$20 km the background winds are from the semi-empirical model of *Groves* [1985,

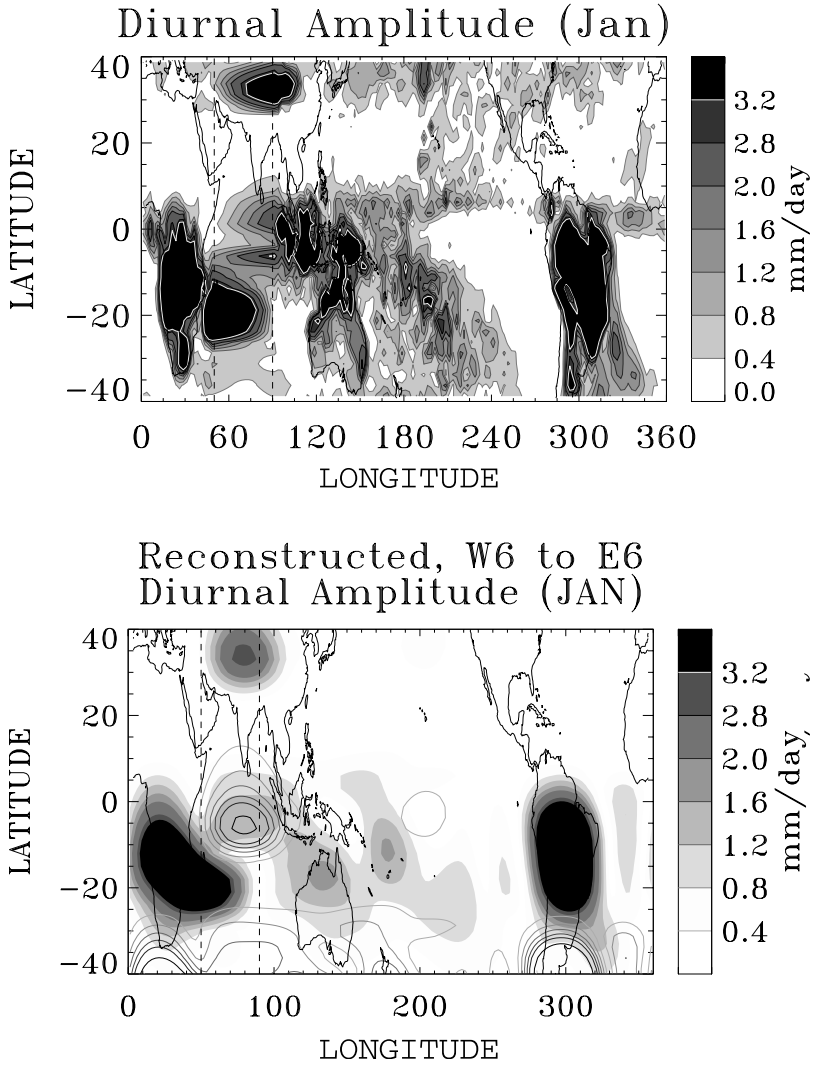

Figure 1. Contours of the diurnal component of rainfall rate (mm/day) deduced from the 7-year GCI measurements made during the months of January (top), and the reconstructed 13 zonal wave number fits (bottom) to these data. See text for details.

1987], but the stratospheric-mesospheric jets and mesopause region winds are based upon Upper Atmosphere Research Satellite (UARS) High Resolution Doppler Interferometer (HRDI) climatologies [*Hagan et al.*, 1999]. Above ~125 km zonal mean zonal winds are from HWM93 [*Hedin et al.*, 1991, 1996].

[10] Dissipation occurs throughout the atmosphere and may be attributable to ion drag, molecular and eddy viscosity and conductivity, and radiative damping. GSWM molecular conductivity and viscosity as well as ion drag and Newtonian cooling parameterizations of radiative damping are discussed by *Hagan et al.* [1993]. GSWM employs a monthly climatology of eddy diffusion coefficients, K_{zz}, and explicitly calculate the divergences of the associated heat and momentum fluxes in the model [cf. *Forbes*, 1982]. K_{zz} account for the effects of turbulence generated by gravity waves as they become unstable and finally break in the upper mesosphere and lower thermosphere (MLT) along with other related mixing phenomena. GSWM K_{zz} are based on the results calculated by *Garcia and Solomon* [1985] as detailed by *Hagan et al.* [1995]. GSWM also includes an effective Rayleigh friction coefficient after *Miyahara and Forbes* [1991] to account for the suppression of the diurnal tide by gravity wave drag [*Hagan et al.*, 1999]. These seasonally variable coefficients were linearly interpolated for the GSWM calculations reported herein.

2.2. GSWM Tidal Forcing Due to Tropospheric Latent Heat Release

[11] In this section we describe our GSWM parameterization of tidal forcing due to latent heat release. We refer the reader to *Forbes et al.* [1997, and references therein] for additional details.

[12] We analyzed 3-hourly measurements of satellite cloud images made during 1988 to 1994. The raw data are infrared cloud brightness temperatures, T, from 40°S to 40°N which are cold when the cloud tops are high and tropical tropospheric convection is deep. The rainfall rate, R_r (mm/hr), can be related to the fractional coverage of clouds (F_c) in a 2.5° latitude by longitude grid box for a

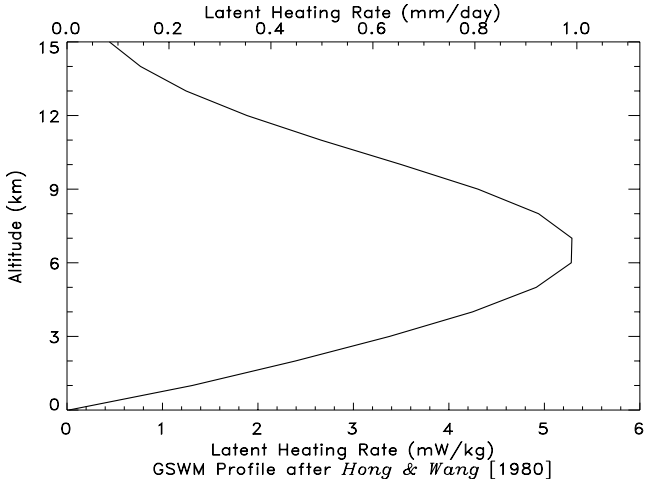

Figure 2. The altitude profile of latent heating rate [after *Hong and Wang*, 1980] invoked in the GSWM parameterization of tidal forcing.

temperature threshold of 235°K [*Arkin and Xie*, 1994; *Janowiak and Arkin*, 1991] as follows:

$$R_r = F_c(T < 235) \bullet 3\left(\frac{mm}{hr}\right). \quad (1)$$

We used this expression to calculate 3-hourly monthly-averaged rainfall rates and then Fourier fit these data at each latitude to quantify the 13 zonal wave number perturbations ($s = -6$, or W6, to $s = 6$, or E6) for both the diurnal and semidiurnal rainfall rate harmonics [*Hendon and Woodberry*, 1993; *Williams and Avery*, 1996] using a function of the form:

$$\sum_{s=-6}^{6}\sum_{n=1}^{2} A_{ns}\cos\left(\frac{2\pi nt}{24} - s\lambda + \Phi_{ns}\right)$$

where n =1(2) for the diurnal (semidiurnal) component, λ is longitude, A_{ns} and Φ_{ns} are the amplitude and phase of the ns component of the fit, respectively.

[13] Figure 1 illustrates a map of the January diurnal rainfall rates that we deduced from the GCI along with our 13-zonal wave number fit to these data. The salient features of the diurnal component of the rainfall are similar to those of the diurnal mean component (not illustrated). Between 50 and 90°E there is a gap in the GCI coverage, so the rainfall rates illustrated at these longitudes are linear interpolations across that gap. As expected during January, rainfall maximizes in the tropical southern hemisphere and over the continents. There are similar patterns for the remaining 11 months, but the rainfall maxima move across the equator with the seasonal migration of the inter-tropical convergence zone (ITCZ). The gross features of the diurnal rainfall rates are also evident in the reconstructed wave number fits (Figure 1). In particular, the fits reproduce the strongest rainfall rates (>3.2 mm/day) over southern Africa and South America. Diurnal rainfall is also very strong (>3.2 mm/day) over Indonesia and Northern Australia and the rates are of order 1–3 mm/day across much of the southern Pacific during January, but there is considerable mesoscale variability at these locations. Thus, the reconstructed fit in this longitude sector (~90–200°E) captures only the large-scale features of the data which results in a significantly smoother pattern that peaks at ~1.6 mm/day. The comparatively weak and less organized precipitation features in the northern hemisphere (e.g., poleward of 10°N) are not represented in the reconstructed fits. Our GSWM tidal forcing parameterization excluded the artifacts of intense rainfall between 30 to 40°N and 90 to 110°E (Figure 1) because they cannot be associated with deep tropical convection. Otherwise, we used these results with an exponential tail-off poleward of 40° to deduce the latitudinal variation of the GSWM diurnal tidal forcing for each zonal wave number.

[14] *Forbes et al.* [1997] illustrated the results of a fast-Fourier transform (FFT) of the related annual average diurnal rainfall rates (their Figure 2) to quantify the large-scale longitudinal variability in the GCI data. They reported the strongest power at $s = -1$, significant contributions at $s = -2$, $s = 0$, and $s = 2$ to $s = 4$, and weaker power at $s = -4$ to $s = -6$. We produced comparable diagnostics (not illustrated) which revealed similar wave number dependencies during all months of the year. These FFT results support our effort to characterize the large-scale longitudinal variability of diurnal latent heat release with 13-zonal wave number fits to the monthly averaged rainfall rates. We note one distinguishing feature of the monthly FFT analysis results. That is, our wave number peaks followed the ITCZ across the equator during the course of the year, while the annual average spectral peaks were nearly hemispherically symmetric [*Forbes et al.*, 1997].

Table 1. GSWM Diurnal Amplitude Maxima: Major Component Responses to Tropospheric Latent Heating

	January	February	March	Apri	May	June	July	August	September	October	November	December
E3 U	*45.5*	*20.5*	*40.0*	*47.4*	5.2	4.1	*23.0*	3.4	*34.1*	*46.1*	*45.9*	*36.8*
E2 U	*19.9*	7.4	*11.0*	8.6	1.9	4.2	3.7	5.2	9.1	*10.4*	*10.6*	*17.0*
W1 U	*14.7*	*21.2*	*29.2*	*24.8*	*22.8*	*15.8*	*16.7*	*22.3*	*26.6*	*35.2*	*24.2*	*17.2*
W2 U	3.1	5.9	5.5	*10.6*	*11.2*	4.9	2.6	3.6	8.2	6.5	8.2	5.6
E3 V	9.4	4.1	*15.5*	8.2	1.5	1.7	6.6	3.0	8.7	8.2	*10.8*	9.0
E2 V	5.4	5.7	*10.6*	4.4	1.7	1.3	3.2	5.0	9.7	*12.5*	7.9	4.9
S0 V	2.1	3.5	8.5	*11.0*	4.9	3.2	2.7	4.2	7.0	*11.3*	6.7	3.1
W1 V	*20.1*	*29.1*	*39.3*	*32.3*	*30.4*	*22.7*	*23.3*	*31.1*	*37.8*	*50.2*	*34.4*	*23.4*
W2 V	4.0	6.8	7.1	*13.4*	*14.0*	7.1	3.4	4.8	*11.5*	9.5	*10.6*	7.4
E3 T	*40.6*	*17.2*	*32.2*	*40.1*	4.4	3.5	*20.9*	2.6	*29.9*	*40.9*	*36.7*	*31.9*
E2 T	*22.3*	7.6	9.8	8.0	1.5	4.4	2.8	3.8	6.5	7.6	9.3	*18.5*
W1 T	9.2	*13.0*	*17.5*	*14.1*	*12.6*	9.7	9.5	*13.9*	*17.0*	*22.8*	*16.0*	*11.0*

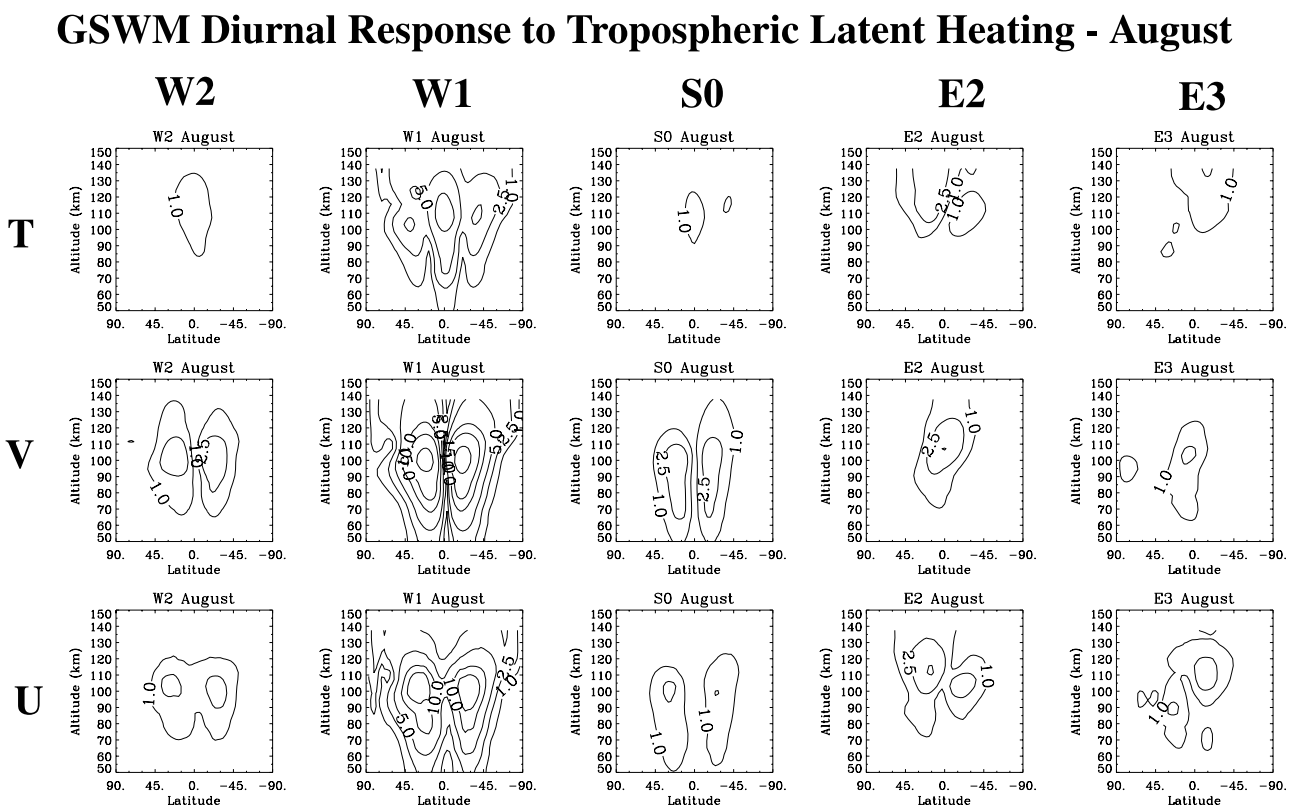

Figure 3. Contours of temperature amplitude (top row; K), meridional (middle row) and zonal (bottom row) wind amplitude (m/s) versus latitude and altitude for the westward 2, migrating, standing, eastward 2 and eastward 3 diurnal tide (left to right columns, respectively) excited by tropospheric latent heat release from GSWM calculations for August.

[15] Figure 2 illustrates $J(z)$, the vertical profile that we employed to complete our GSWM specification of the tidal forcing due to tropospheric latent heating:

$$J(z) = 5.34\frac{\mathrm{mW}}{\mathrm{kg}}\left\{\exp\left[-\left(\frac{z-6.5}{5.39}\right)^2\right] - 0.23\exp\left(\frac{-z}{1.31}\right)\right\} \quad (2)$$

Equation (2) was initially developed by *Hong and Wang* [1980] for altitude, z (km), and 1.0 mm/day =5.34 mW/kg. $J(z)$ peaks at 6.5 km, but it can only be associated with deep convective activity since the heating extends throughout the troposphere; from the surface up to an altitude that is consistent with the global-mean tropopause. Our GCI rainfall determinations inherently include elements of the so-called stratiform precipitation which forms in comparatively narrow layers in the tropical troposphere [*Houze*, 1997]. Thus, we reduced the monthly rainfall rates by 25% to exclude stratiform precipitation effects from our GSWM tidal forcing scheme in keeping with the discussion put forth by *Houze* [1997].

[16] The depth of the heating specified by equation (2) and illustrated in Figure 2 suggests that diurnal tidal components with vertical wavelengths of ~25–30 km should be readily excited by this forcing function [e.g., *Garcia and Salby*, 1987]. Because the upward propagating migrating diurnal tide has such a vertical wavelength and the GCI FFT analysis revealed strong signatures of an $s = -1$ diurnal component, it is reasonable to expect that deep convective activity in the tropical troposphere generates a migrating diurnal tide that propagates into the middle and upper atmosphere during every month of the year. In the following section we report on the GSWM calculations that confirm this conjecture and investigate the associated nonmigrating diurnal tides that, along with the monthly variable zonal mean zonal winds and dissipation, modulate the behavior of the migrating component.

3. Results

3.1. Major Component Solutions

[17] We calculated the diurnal tidal response for each of 13 zonal wave numbers ($s = -6$ to $s = 6$) and for every month of the year using the aforementioned background atmosphere and tidal forcing and dissipation schemes. In this section we overview the GSWM solutions, and describe and illustrate representative results for April and August in some detail.

[18] Due to space limitations it is impossible for us to discuss herein the entire set of 156 diurnal calculations that we performed. We focus therefore on the subset of GSWM solutions with MLT temperature perturbations, $T \geq 10°K$, zonal wind perturbations, $U \geq 10$ m/s, or meridional wind perturbations, $V \geq 10$ m/s, during at least one month of the year. Hereafter, we refer to these components of the diurnal tide excited by tropospheric latent heat release as the major components. They include the eastward propagating zonal wave number 3 (E3), the eastward propagating zonal wave

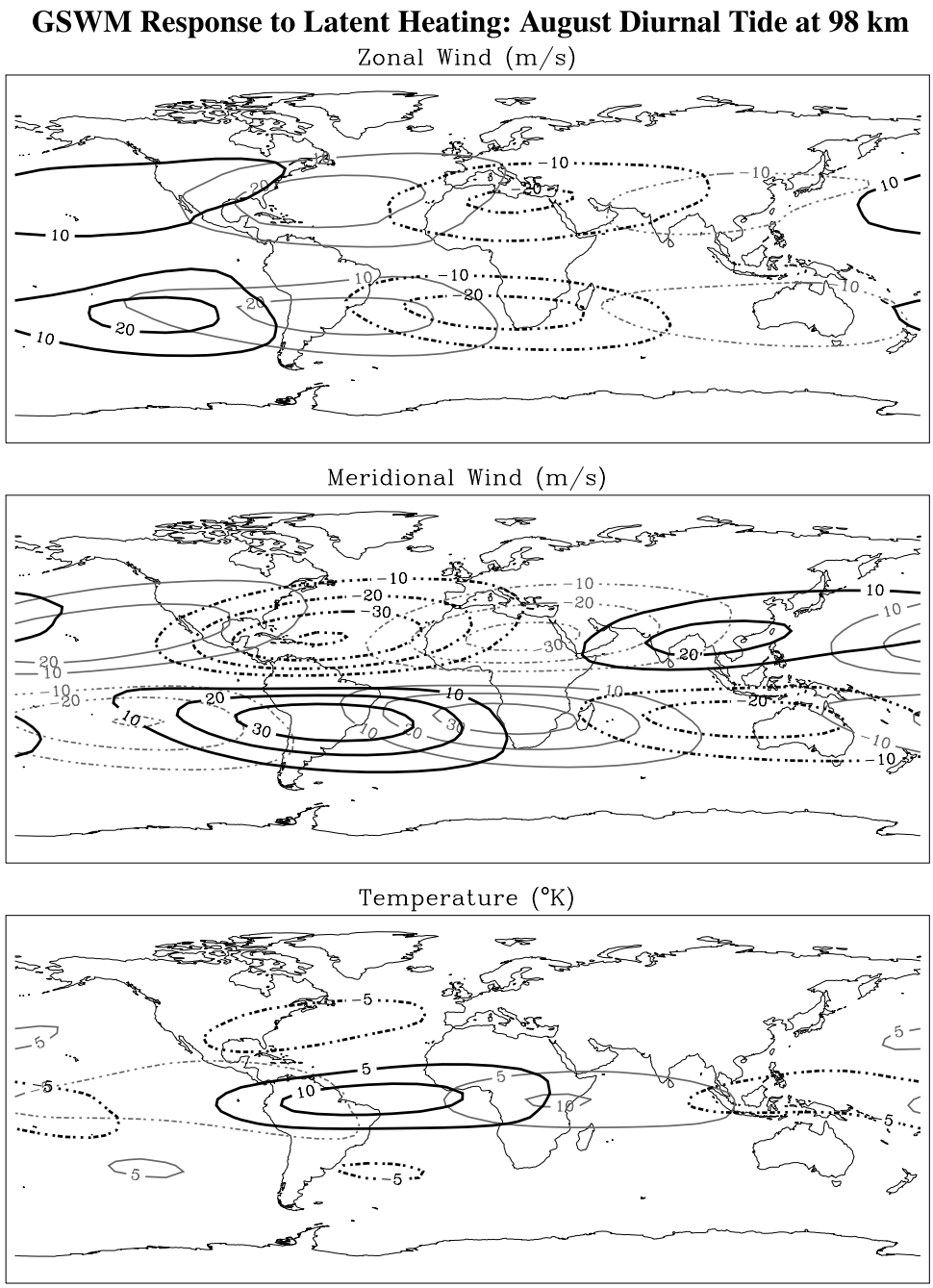

Figure 4. Contours of the GSWM 98-km diurnal tidal perturbations at 12 UT (black) and 06 UT (gray) versus longitude and latitude during August. The zonal wind (top), meridional wind (middle), and temperature (bottom) perturbations (positive: solid and negative: dot-dash) include the combined effects of the W1, W2, S0, E2, and E3 components excited by tropospheric latent heating. See text for details.

number 2 (E2), the standing zonal wave number 0 (S0), the westward propagating zonal wave number 2 (W2), and the westward propagating zonal wave number 1 (W1) or migrating diurnal tides.

[19] Table 1 is a catalog of the major component results from our GSWM calculations for each month of the year. Therein, we tabulate the GSWM zonal, meridional, and temperature amplitude maxima as a function of diurnal component and month. We also italicize the amplitude maxima that meet the aforementioned $T \geq 10°K$, $U \geq 10$ m/s, and $V \geq 10$ m/s criteria. As expected, the most persistent MLT response to deep diurnal latent heating in the troposphere is that of the W1 migrating component. W1 U maxima range between about 15 and 35 m/s; V between 20 and 50 m/s; and, T between 9 and 23°K. The migrating diurnal component is largest during October and smallest during January with secondary maxima and minima in March and June, respectively. This seasonal variability is also typical of the MLT response of the migrating diurnal tide that is excited by the absorption of solar radiation and affected by monthly variable dissipation [e.g., *Hagan et al.*, 1999], but there are differences in the details. During every

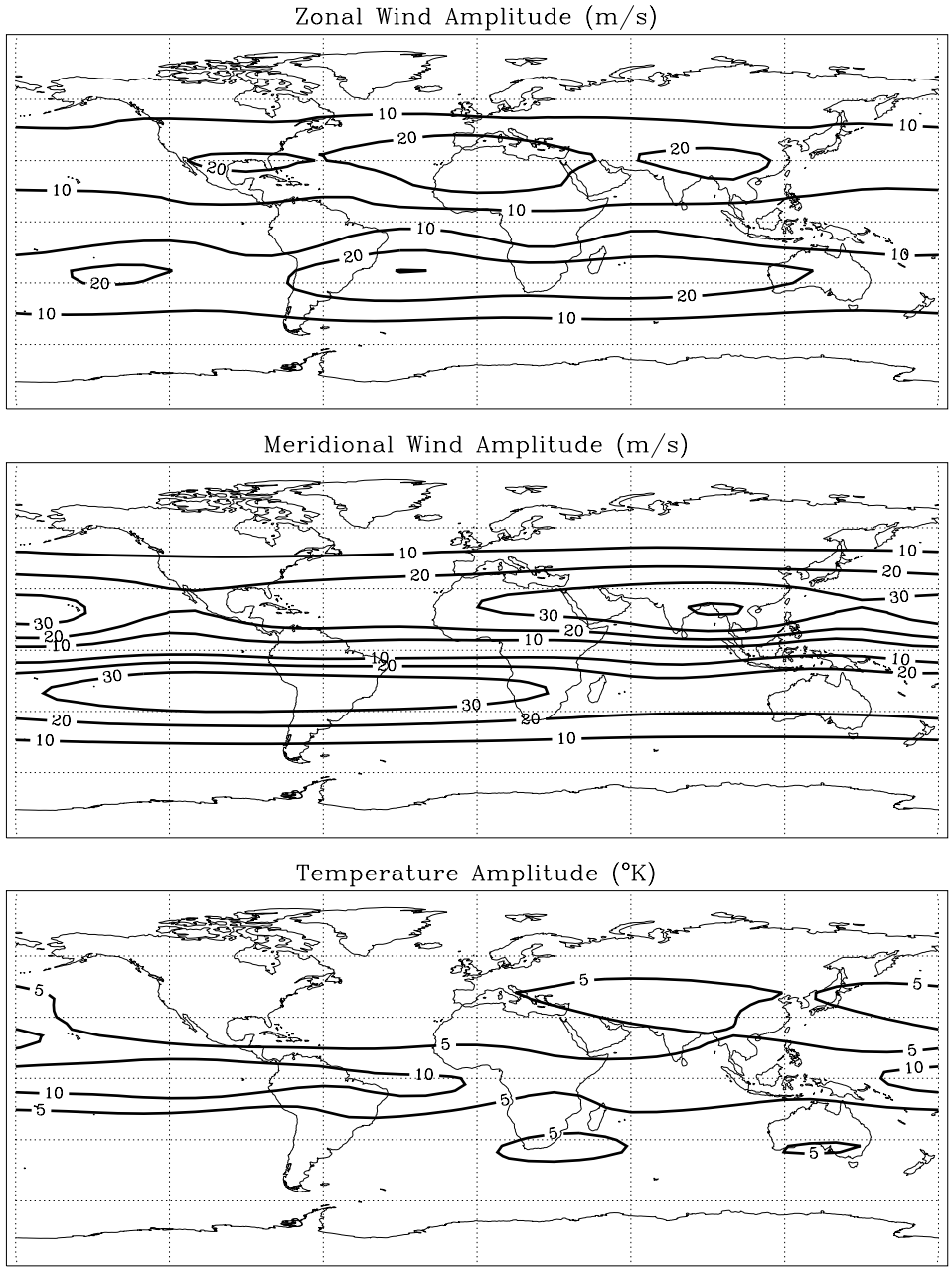

Figure 5. Contours of diurnal zonal (top) and meridional (middle) wind and temperature (bottom) amplitude from GSWM calculations of the W1, W2, S0, E2, and E3 tides excited by latent heat release in the troposphere during August. See text for details.

month of the year the GSWM radiative response is larger than the latent heating response. The radiative maxima are of comparable magnitudes near equinox, while the latent heating response is some 20 to 25% larger in October than in March. Further, the April radiative response is larger than the March response, while the reverse is true for the latent heating solutions (Table 1).

[20] Although the W1 diurnal tide is the most persistent major component of the GSWM latent heating solutions, the E3 U and T amplitude maxima exceed the W1 U and T maxima during nine months of the year (Table 1). The exceptions include May, June, and August when the E3 U $\leq$ 5 m/s and T < 5°K. The E2 diurnal tide is also a major component of the MLT response. The E2 U and T responses are greater than or comparable to the W1 tide during December and January, and these E2 amplitude maxima are also significant during March, October, and November. Both the E3 and E2 components are diurnal Kelvin waves; their V response is weaker than their U and T responses.

[21] The W1, E3, and E2 are the major components of the GSWM diurnal temperature response to tropospheric latent heating, but additional components significantly affect the aggregate horizontal wind solutions in the MLT (Table 1). Specifically, the W2 tide meets both the U $\geq$ 10 m/s and V $\geq$

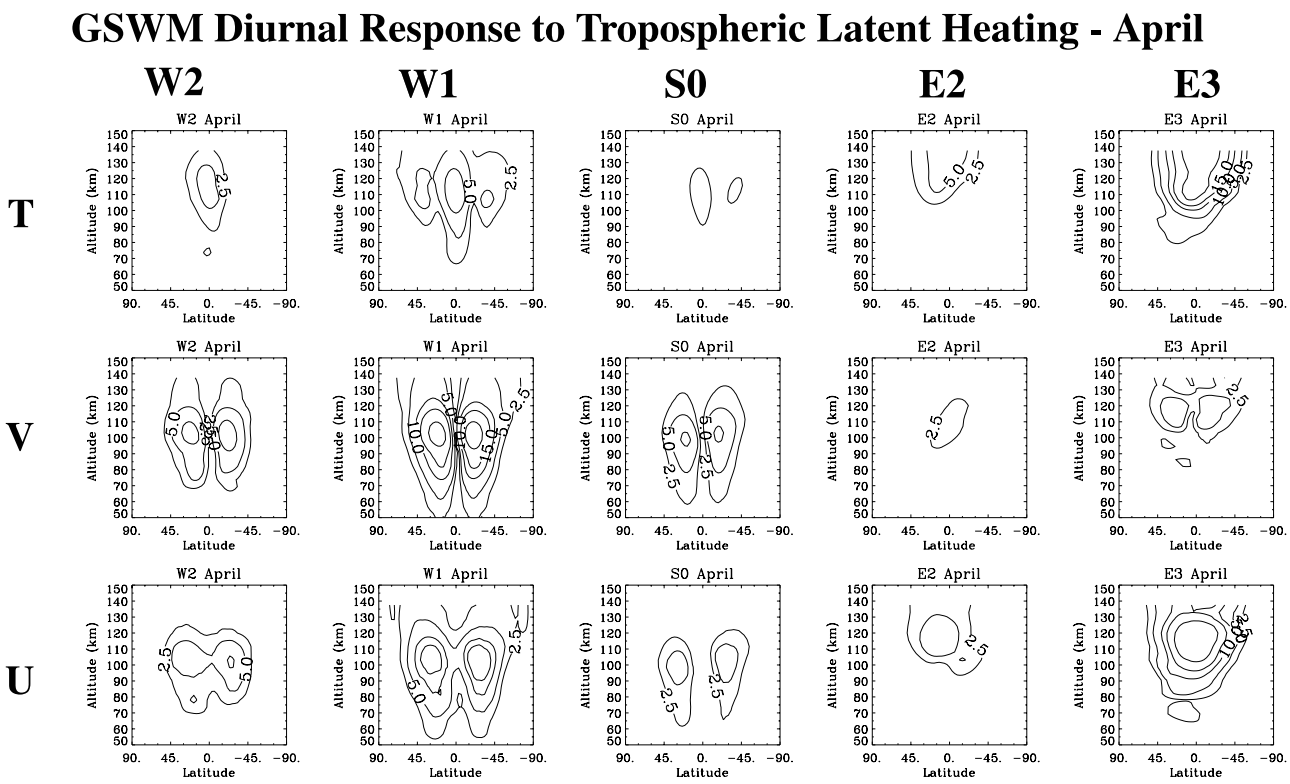

Figure 6. Same as Figure 3 except for April.

10 m/s criteria during April and May. W2 V$\geq$10 m/s during September to November as well. Finally, the S0 V further influences the meridional MLT response during both April and October.

[22] The magnitude of major component amplitude maxima (Table 1) provide neither perspective on the latitudinal and altitudinal structure of the GSWM diurnal tidal solutions, nor insight into the comparative importance of the various diurnal component contributions at a particular location. In the following sections, we present our major component solutions for April and August to further characterize the GSWM response to deep convection in the troposphere. The nonmigrating diurnal tidal responses are strong during April and weak during August (Table 1). Thus, these results are representative of some of the characteristics of the seasonal variability of the nonmigrating diurnal tides due to latent heat release.

3.2. August Results

[23] We focus first on the GSWM August results, because the MLT solutions are dominated by the behavior of the most familiar migrating component. Figure 3 illustrates contours of T, U, and V as a function of latitude and altitude in the middle and upper atmosphere during April for each of the 5 major components of the diurnal tide that we identified in the previous section (Table 1). The W2, S0, E2, and E3 solutions are very weak with peak V and U $\leq$ 5 m/s and T $\leq$ 5°K. The W1 component response is strong (Table 1 and Figure 3) and it exhibits latitudinal and altitudinal variations that are consistent with those of the migrating diurnal tide excited by the absorption of solar radiation in the troposphere, stratosphere and mesosphere [e.g., *Hagan et al.*, 1999]. That is, temperature amplitudes peak near $\sim$112 km over the equator, while zonal and meridional wind amplitudes approach zero near the equator and maximize at $\sim$98–104 km near $\pm$30° and $\pm$20°, respectively.

[24] Figure 4 is a 12 UT snapshot of the collective W2, W1, S0, E2, and E3 diurnal tide at 98 km with the shadow of the corresponding 06 UT diurnal tidal snapshot. The U, V, and T perturbation contours all exhibit the features of a wave number 1 oscillation which propagates westward between the snapshots. The expected W1 phase behavior is also evident. Specifically, northern and southern hemisphere zonal wind perturbations are phase coherent, while the equivalent meridional wind perturbations are out of phase. The low latitude secondary temperature maxima are out of phase with the equatorial perturbations. Even though the morphology of the GSWM 98-km diurnal response during August is dominated by the W1 tide, there is also evidence of the collective effects of the 4 major nonmigrating components in Figure 4. The structure and intensity of the perturbation maxima evolves between 06 and 12 UT.

[25] Figure 5 provides further evidence of the W2, S0, E2, and E3 effects on the aggregate GSWM August solution. The U, V, and T diurnal tidal amplitudes at 98 km all vary with longitude which distinguishes them from the pure migrating perturbations which are longitude invariant (not illustrated). At a given latitude diurnal temperature amplitudes vary with longitude by up to $\sim$10°K at 98 km. Corresponding zonal and meridional wind variations are of order 10 m/s and 20 ms, respectively. The pattern of U, V, and T longitude variations is complicated and not coherent. For example, the zonal wind amplitudes are comparatively small over the Pacific at northern and, to a lesser extent southern, low latitudes. But, the comparatively small meri-

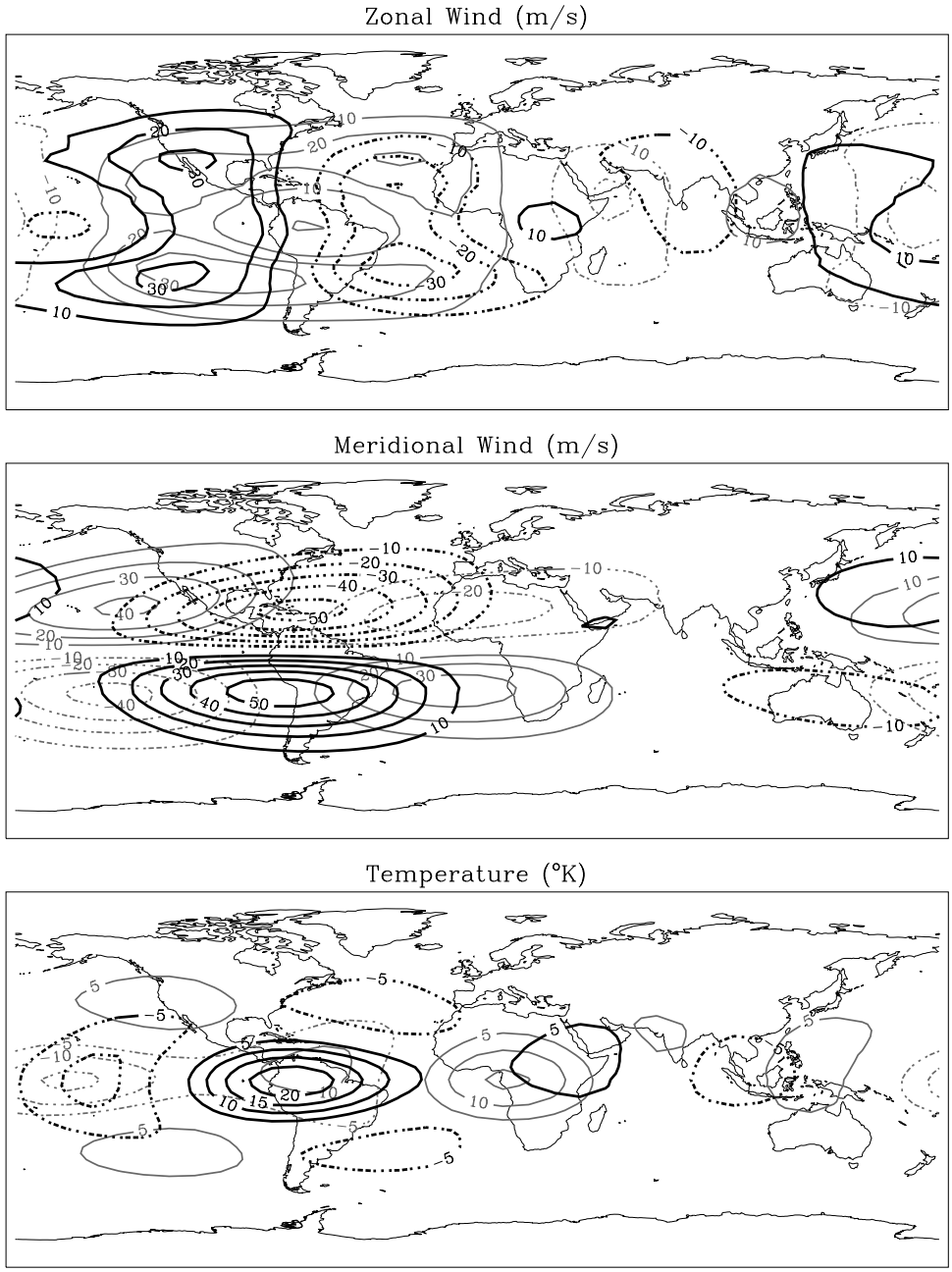

Figure 7. Same as Figure 4 except for April.

dional amplitudes are located over Australia, and the northern Atlantic and Indian Oceans.

3.3. April Results

[26] The major nonmigrating tidal component amplitudes are much larger during April (Figure 6) than August (Figure 3), while the migrating component responses are comparable (Table 1). The salient features of the W2 and S0 diurnal tide are similar to the W1 migrating component with temperature amplitude peaks near ~112 km over the equator, and zonal and meridional wind amplitude peaks at low latitudes near ~98–104 km. The structure of the E2 and E3 diurnal Kelvin waves is dramatically different. Both U and T peak over the equator at some 10–20 km above the remaining component peaks. The comparatively weak E3 V has double peaks that are in excess of 5 m/s. This response also peaks ~10 km higher than, and has a much broader altitudinal structure than the W1 V, W2 V, and S0 V. There is some hemispheric asymmetry associated with all of the illustrated solutions which is attributable to the combined effects of the background zonal winds and the tidal dissipation in the GSWM.

[27] The 98-km 12 UT collective migrating and nonmigrating diurnal snapshot is illustrated in Figure 7 with the consonant 06 UT snapshot shadow resulting from the GSWM April calculations. The nonmigrating components (Figure 6) significantly modulate the migrating tide during April as evidenced in the combined diurnal response of U,

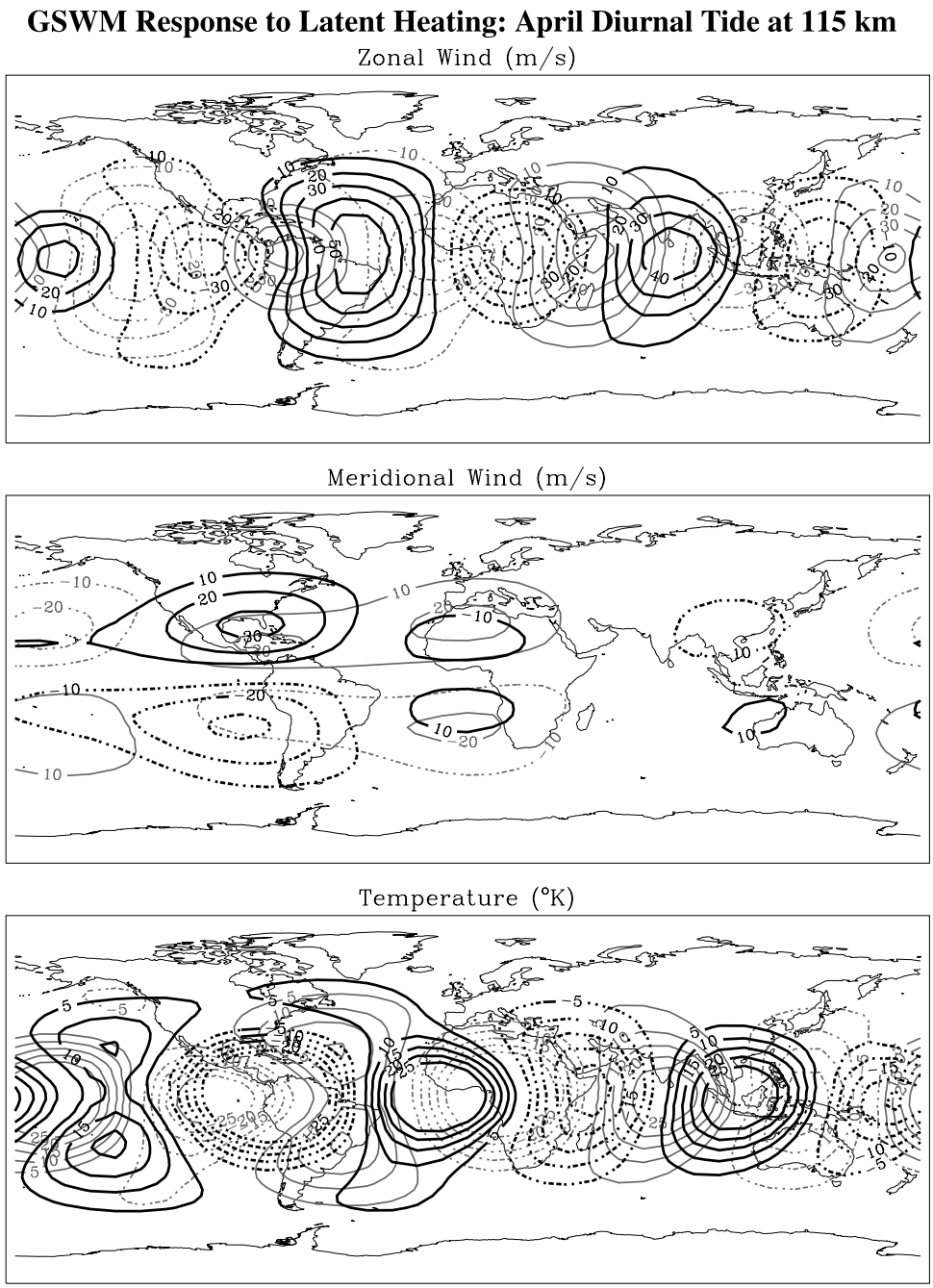

Figure 8. Same as Figure 7 except for 115 km.

V, and T (Figure 7). Despite some distortion of the wave number 1 pattern, the 06 UT diurnal V response is similar to the corresponding August result (Figure 4), but the evolution of the comparatively strong nonmigrating V tides renders the 12 UT patterns very different. Specifically, the peak variations are enhanced over the Americas and they almost disappear from the Asian and Australian sector. The differences between the April and August U and T responses are more dramatic, because the E3 diurnal Kelvin wave amplitudes are comparable to the migrating components at 98 km in April (Figure 6). This wave produces strong U variations over the equator and a distorted wave number 3 pattern in both the aggregate T and U 12 UT responses, but not in the 06 UT response. The collective response of the 06 and 12 UT GSWM diurnal tidal fields suggests that tropospheric latent heating during April yields perturbations that evolve significantly as they propagate with longitude at 98 km. Therefore, there are strong variations in the collective diurnal tidal amplitude with longitude (not illustrated) associated with the combined migrating and nonmigrating 98-km results.

[28] Figure 8 illustrates the snapshots that are comparable to Figure 7 except they represent the aggregate GSWM perturbations at 115 km where the E3 component dominates the diurnal tidal response during April (Figure 6). As expected, both the U and T fields exhibit clear wave number 3 signatures which propagate eastward. These wave patterns evolve primarily in response to the W1 and E2 contributions

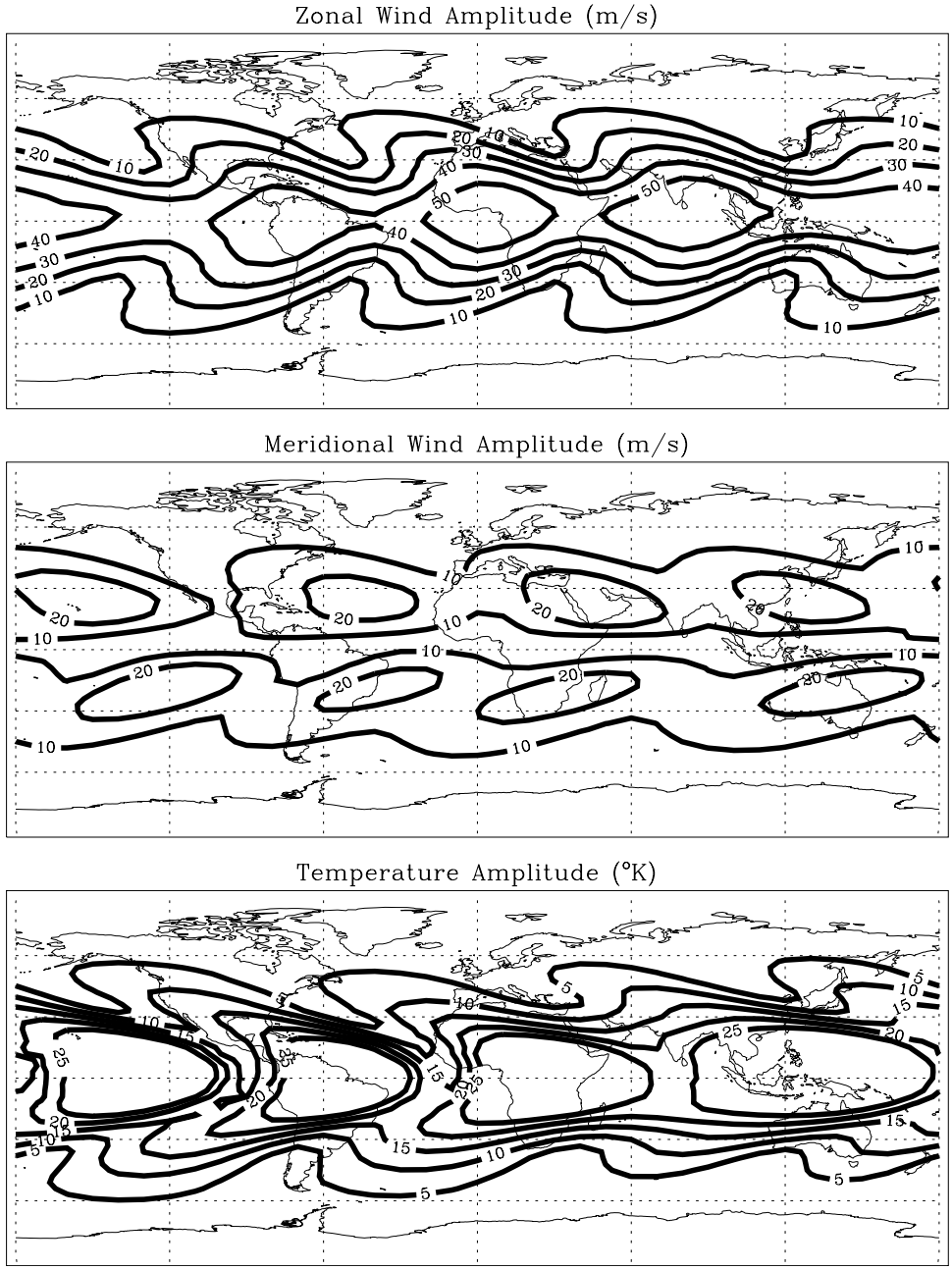

Figure 9. Same as Figure 5 except for April results at 115 km.

which are of comparable magnitudes at 115 km. Not surprisingly, the diurnal V response is considerably different given that the migrating component is dominant and modulated by the W2, E3, and S0 nonmigrating V tides. The corresponding amplitude variations are illustrated in Figure 9. To first order, the U and T diurnal tides excited by latent heating look symmetric about the equator, while there are interhemispheric asymmetries in the V tide that are as large as 10 m/s (e.g., in the Hawaiian longitude sector).

3.4. Month to Month Variations at Select Latitudes and Altitudes

[29] In our discussion of Table 1 we noted that the comparative importance of the component responses to diurnal tropospheric latent heat forcing varies significantly from month to month. In this section we quantify this variability for select diurnal components that dominate the aggregate tidal responses at 98 and 115 km.

[30] Figure 10 illustrates the month to month variations of the 98-km migrating (i.e., W1) U, V, and T amplitudes and phases at select latitudes. The differences between the ±30°U and ±20°V results quantify the interhemispheric asymmetries at latitudes near their respective 98-km peak responses (Figures 3 and 6), while the equatorial wind results represent the maximum T and minimum U and V migrating tidal responses at low and middle latitudes. The monthly variations in the peak amplitudes that we previously discussed (Section 3.1; Table 1) are evident in the 98-km migrating diurnal amplitudes. The ±30°U, ±20°V, and equatorial T amplitudes vary semiannually with relative maxima during

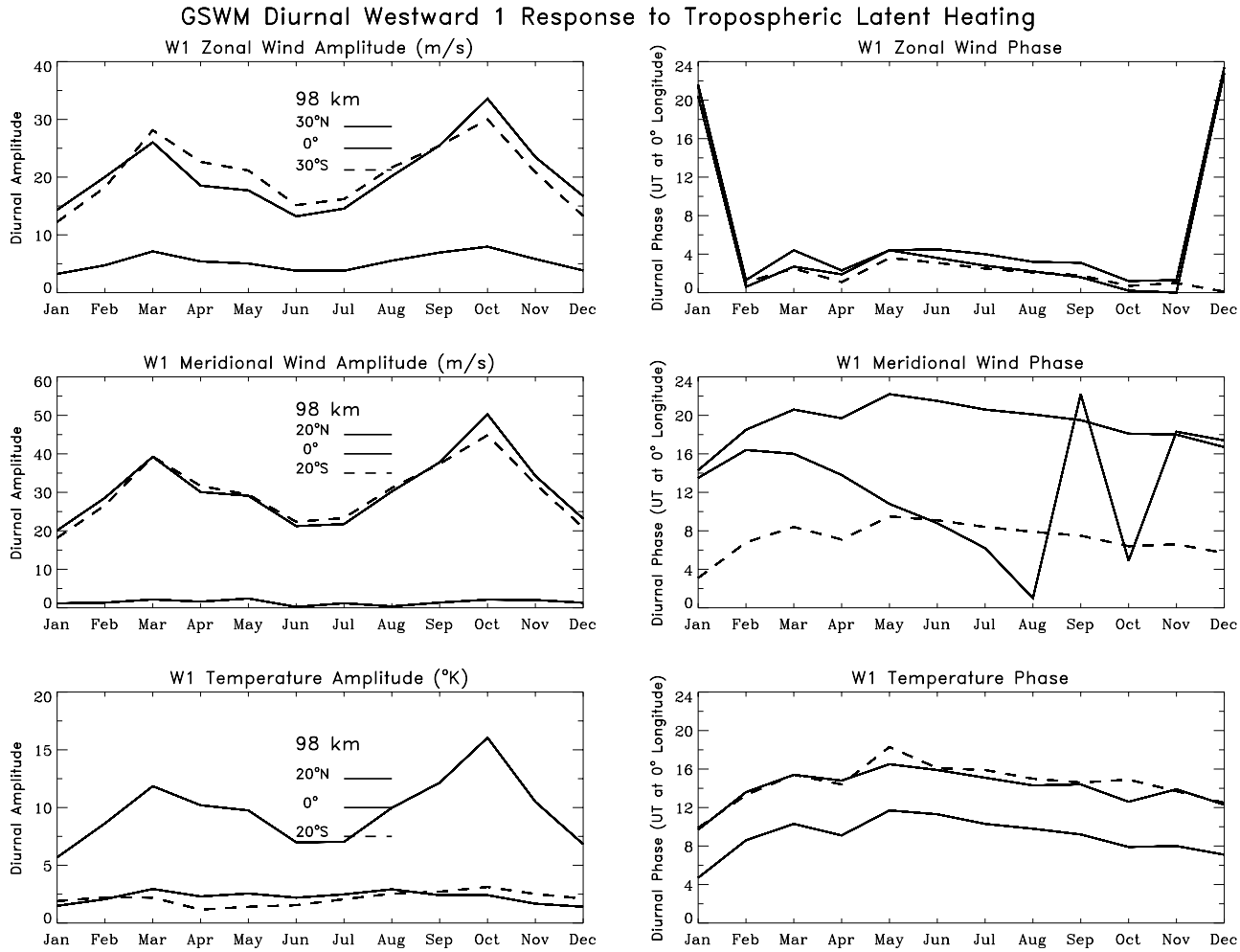

Figure 10. GSWM equatorial (dash-dot) migrating diurnal zonal (top), meridional (middle), and temperature (bottom) amplitudes (left) and phases (right) at 98 km versus month. ±30° migrating diurnal zonal winds (solid and dashed curves, respectively) are also illustrated with ±20° meridional winds and temperatures (solid and dashed curves, respectively).

April and October and minima during June–July and December–January. October amplitudes are larger than April amplitudes. The equatorial U and ±20°T amplitudes are small (∼5 m/s; ∼5°K) with barely discernible variations of order 1–2 m/s and 1–2°K, respectively. At locations where there are significant amplitudes (i.e., all except the 0°V response) the migrating diurnal phase variations appear to be largely annual. That is, diurnal phases shift smoothly by up to +6 UT hours between January and May and then gradually shift back during June to December. The ±30° U phases are coherent, while the 20°N V phases lead their ±20°S counterparts by 12 hours. There is a ∼+6 UT hour shift between the T phases over the equator and those at ±20°. These phase relationships are consistent with those of the migrating diurnal tide that is radiatively forced in the Earth's atmosphere [e.g., *Hagan et al.*, 1999].

[31] The month to month variations of the E3 diurnal tide at 115 km are illustrated in Figure 11. U, V, and T E3 results are shown for the identical latitudes discussed above and illustrated in Figure 10, but in contrast to the results for the W1 tide, there is a broad U and T E3 amplitude peak centered over the equator (e.g., Figure 6) that persists throughout most of the year (Figure 11). The exceptions are the months of May, June and August, when no appreciable E3 component is present in the GSWM solutions near 115 km. The corresponding U and T phases are coherent with latitude between the equator and ±20 to ±30°, but they exhibit month to month variations which are noteworthy when the amplitudes are sufficiently large that the corresponding phases are well defined. The amplitudes are small between June and August when the phase shifts by 11 to 12 UT-hours to later times. During the remainder of the year the phases are well defined and characterized by a gradual −2 to 3 UT-hour shift between August and December followed by a gradual +2 to 3 UT-hour shift between January and April. Between April and June the phases rapidly shift back in time again by ∼12 UT hours. The month to month variations of the E3 V amplitudes and phases are comparatively less well organized than those of the U and T components. The salient features of the monthly V amplitude variability is similar to the U and T components, but the peak response is not centered over the equator (e.g., Figure 6). There is also more V phase variability as compared with U and T, but the corresponding amplitudes are also considerably smaller.

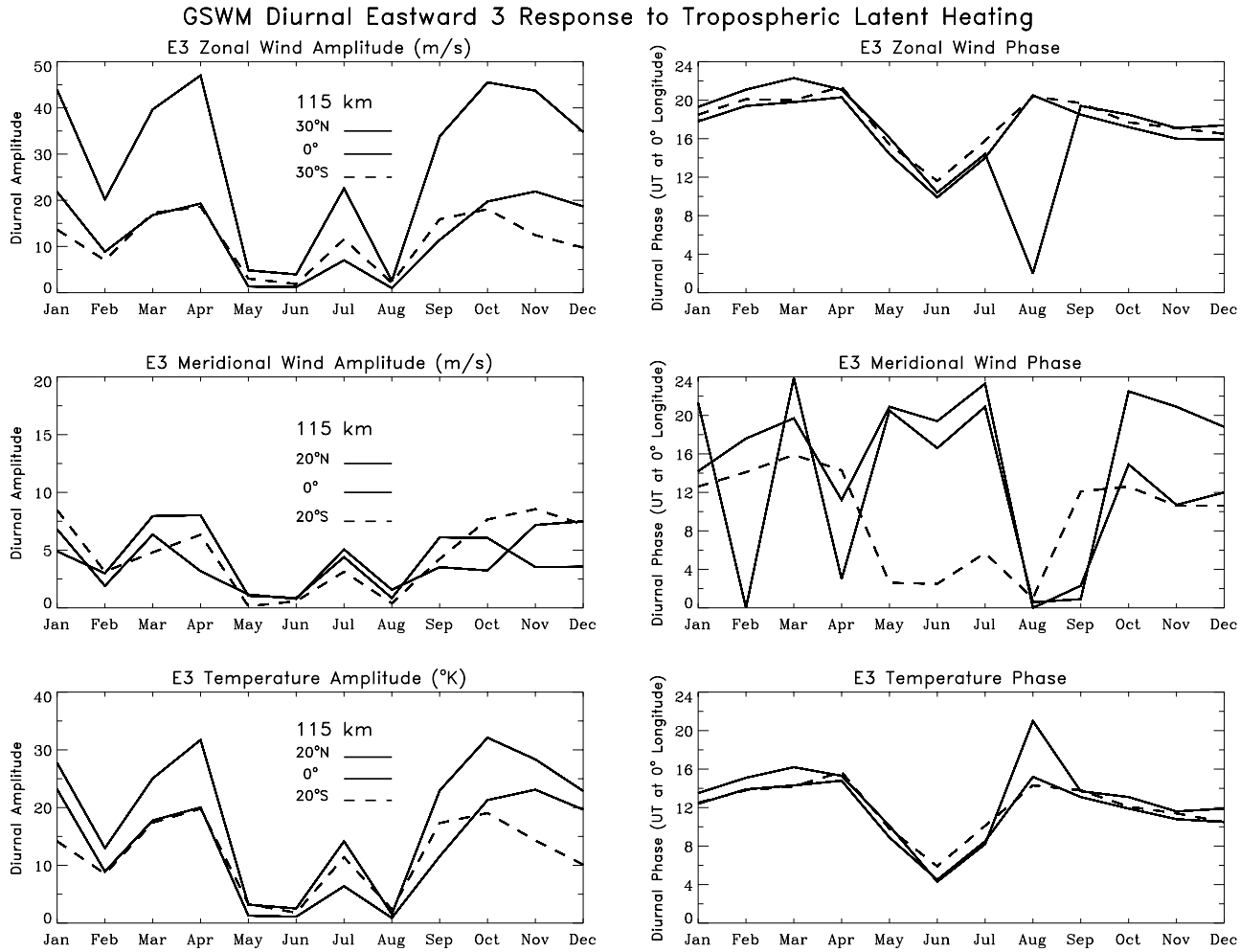

Figure 11. Same as Figure 10 except for the nonmigrating eastward 3 diurnal results at 115 km.

[32] The seasonal variability of the GSWM MLT migrating and nonmigrating diurnal tides is attributable to the combined effects of the mean winds that we assume in our calculations along with our forcing and dissipation parameterizations. *Burrage et al.* [1995] and later *Hagan et al.* [1999] reported on the GSWM numerical experiments that quantified the respective roles of these effects on the radiatively excited migrating diurnal component. Although they reported that stratospheric and lower mesospheric zonal mean zonal winds affect the MLT amplitudes by up to 30%, these studies suggest that the GSWM gravity wave stress parameterization has the most profound effect on the diurnal MLT response. The fundamental questions about whether and how gravity waves accelerate or decelerate the diurnal tide [*McLandress*, 1998; *Mayr et al.*, 1998; *Meyer*, 1999], and to what extent nonlinear interactions between the migrating diurnal tide and planetary waves further affect the tide in the MLT [*McLandress*, 1997; *Norton and Thuburn*, 1999; *Hagan and Roble*, 2001] remain unresolved, but the seasonal variability of the MLT migrating diurnal tide is firmly established [e.g., *Vincent et al.*, 1989; *Burrage et al.*, 1995; *McLandress et al.*, 1996]. In order to reproduce this variability, GSWM calculations of the radiatively driven migrating diurnal tide include a linear damping (Rayleigh friction) coefficient in the momentum equations [e.g., *Hagan et al.*, 1995, 1999, 2001]. This empirical treatment is justified in a mechanistic modeling approach, because the physics of the wave-tide interactions is not understood. Upward propagating migrating and nonmigrating diurnal tidal components have comparable vertical wavelengths and horizontal scales, so we also included these effects in the GSWM calculations that we report herein. Specifically, we linearly interpolated the seasonally variable Rayleigh friction coefficients that are detailed by *Hagan et al.* [1999] to introduce monthly variability in our calculations. Thus, the month-to-month variability of the GSWM response to tropospheric latent heating (Table 1; Figures 10 and 11) requires future observational verification. In particular, we need further observational diagnostics to assess whether the GSWM is accurately predicting the longitudinal variability of the diurnal tide in the MLT and whether the linear damping that we invoked in our calculations continues to be viable.

4. Summary and Conclusions

[33] We used seven years of global cloud imagery data representing geographical locations of deep convective activity to parameterize tropospheric latent heating rates. We decomposed the rates into 2 harmonic and 13 zonal

wave number components for each month of the year [after *Forbes et al.*, 1997]. We subsequently used these data in a series of GSWM calculations to explore the effects on the associated migrating and nonmigrating diurnal and semidiurnal tidal signatures aloft. Herein, we report on the diurnal results which suggest that the aggregate effects of the latent heating source vary from month to month and produce measurable diurnal amplitude variations ($\sim$10–20 m/s and 5–15°K) at select low and middle latitude locations in the upper atmosphere. Thus, tropospheric latent heating may be an important source of tidal variability in the mesosphere and lower thermosphere and may partly explain differences between tidal signatures measured at the ground and those inferred from space-based measurements.

[34] Our result suggests that in order to produce realistic longitudinal diurnal tidal variability, dynamical models need to account for the tropospheric latent heat source. Since the tropospheric latent heating produces a MLT diurnal response that modulates the migrating tide excited by the absorption of solar radiation [e.g., *Hagan et al.*, 1997a], the GSWM results we present herein must be combined with the complementary GSWM radiative solutions [e.g., *Hagan et al.*, 2001] to produce monthly climatologies of the diurnal tide. These combined results should be evaluated by examining diurnal tidal signatures deduced from longitudinal radar and optical instrument chains at a series of latitudes, from satellite measurements of MLT winds and temperatures, and from combined ground-based and satellite data sets. The partnership between the CEDAR and TIMED communities and the international PSMOS efforts present invaluable opportunities for further observational studies of migrating and nonmigrating diurnal tides in the Earth's middle and upper atmosphere. GCM researchers can extend our efforts and quantify how the nonmigrating components excited by nonlinear interactions may further modulate the latent heat responses that we discuss herein.

[35] **Acknowledgments.** The authors thank M. Wheeler for valuable discussions about convective and stratiform precipitation. We also thank R. Roble for comments on an initial draft of this manuscript and X. Zhang for preparing Figure 1 and the tabulations of monthly tidal heating rates. The National Center for Atmospheric Research (NCAR) is sponsored by National Science Foundation (NSF). M. Hagan acknowledges the support of the NSF CEDAR program, the National Aeronautics and Space Administration (NASA) Sun-Earth Connections Theory Program, and grant S-S-10105X to NCAR. J. Forbes acknowledges support from the NSF through grant ATM-0097829 to the University of Colorado.

References

Arkin, P. A., and P. P. Xie, The global precipitation climatology project: First algorithm intercomparison project, *Bull. Am. Meteorol. Soc.*, *75*, 401–419, 1994.

Burrage, M. D., M. E. Hagan, W. R. Skinner, D. L. Wu, and P. B. Hays, Long-term variability in the solar diurnal tide observed by HRDI and simulated by the GSWM, *Geophys. Res. Lett.*, *22*, 2641–2644, 1995.

Chapman, S., and R. S. Lindzen, *Atmospheric Tides*, 201 pp., D. Reidel, Norwell, Mass., 1970.

Ekanayake, E. M. P., T. Aso, and S. Miyahara, Background wind effect on propagation of nonmigrating diurnal tides in the middle atmosphere, *J. Atmos. Sol. Terr. Phys.*, *59*, 401–429, 1997.

Forbes, J. M., Atmospheric tides, 1, Model description and results for the solar diurnal component, *J. Geophys. Res.*, *87*, 5222–5240, 1982.

Forbes, J. M., Middle atmosphere tides, *J. Atmos. Terr. Phys.*, *46*, 1049–1067, 1984.

Forbes, J. M., Tidal and planetary waves, in *The Upper Mesosphere and Lower Thermosphere: A Review of Experiment and Theory, Geophys. Monogr. Ser.*, vol. 87, edited by R. M. Johnson and T. L. Killeen, pp. 67–87, AGU, Washington, D. C., 1995.

Forbes, J. M., and H. B. Garrett, Theoretical studies of atmospheric tides, *Rev. Geophys.*, *17*, 1951–1981, 1979.

Forbes, J. M., and G. V. Groves, Diurnal propagating tides in the low-latitude middle atmosphere, *J. Atmos. Terr. Phys.*, *49*, 153–164, 1987.

Forbes, J. M., M. E. Hagan, X. Zhang, and K. Hamilton, Upper atmospheric tidal oscillations due to latent heat release in the tropical troposphere, *Ann. Geophys.*, *15*, 1165–1175, 1997.

Garcia, R. R., and M. L. Salby, Transient response to localized episodic heating in the tropics, part II, Far-field behavior, *J. Atmos. Sci.*, *44*, 499–530, 1987.

Garcia, R. R., and S. Solomon, The effect of breaking gravity waves on the dynamics and chemical composition of the mesosphere and lower thermosphere, *J. Geophys. Res.*, *90*, 3850–3868, 1985.

Groves, G. V., A global reference atmosphere from 18 to 80 km, *AFGL Tech Rep., TR-85-0129*, 1985.

Groves, G. V., Final scientific report, *AFOSR Rep. 84-0045*, Air Force Off. of Sci. Res., Bolling Air Force Base, Washington, D.C., 1987.

Hagan, M. E., Comparative effects of migrating solar sources on tidal signatures in the middle and upper atmosphere, *J. Geophys. Res.*, *101*, 21,213–21,222, 1996.

Hagan, M. E., Atmospheric tidal propagation across the stratopause, *Atmospheric Science Across the Stratopause, Geophys. Monogr. Ser.*, vol. 123, edited by D. E. Siskind, S. D. Eckermann, and M. E. Summers, pp. 177–190, AGU, Washington, D. C., 2000.

Hagan, M. E., and R. G. Roble, Modeling diurnal tidal variability with the National Center for Atmospheric Research thermosphere–ionosphere–mesosphere–electrodynamics general circulation model, *J. Geophys. Res.*, *106*, 24,869–24,882, 2001.

Hagan, M. E., J. M. Forbes, and F. Vial, A numerical investigation of the propagation of the quasi 2-day wave into the lower thermosphere, *J. Geophys. Res.*, *98*, 23,193–23,205, 1993.

Hagan, M. E., J. M. Forbes, and F. Vial, On modeling migrating solar tides, *Geophys. Res. Lett.*, *22*, 893–896, 1995.

Hagan, M. E., J. L. Chang, and S. K. Avery, GSWM estimates of nonmigrating tidal effects, *J. Geophys. Res.*, *102*, 16,439–16,452, 1997a.

Hagan, M. E., C. McLandress, and J. M. Forbes, Diurnal tidal variability in the upper mesosphere and lower thermosphere, *Ann. Geophys.*, *15*, 1176–1186, 1997b.

Hagan, M. E., M. D. Burrage, J. M. Forbes, J. Hackney, W. J. Randel, and X. Zhang, GSWM-98: Results for migrating solar tides, *J. Geophys. Res.*, *104*, 6813–6828, 1999.

Hagan, M. E., R. G. Roble, and J. Hackney, Migrating thermospheric tides, *J. Geophys. Res.*, *106*, 12,739–12,752, 2001.

Hamilton, K., Latent heat release as a possible forcing mechanism for atmospheric tides, *Mon. Weather Rev.*, *109*, 3–17, 1981.

Hedin, A. E., Extension of the MSIS thermosphere model into the middle and lower atmosphere, *J. Geophys. Res.*, *96*, 1159–1172, 1991.

Hedin, A. E., et al., Revised global model of thermosphere winds using satellite and ground-based observations, *J. Geophys. Res.*, *96*, 7657–7688, 1991.

Hedin, A. E., et al., Empirical wind model for the upper, middle, and lower atmosphere, *J. Atmos. Terr. Phys.*, *58*, 1421–1447, 1996.

Hendon, H. H., and K. Woodberry, The diurnal cycle of tropical convection, *J. Geophys. Res.*, *98*, 16,623–16,637, 1993.

Hong, S.-S., and P.-H. Wang, On the thermal excitation of atmospheric tides, *Bull. Geophys. Natl. Cent. Univ. Taiwan,*, *19*, 56–83, 1980.

Houze, R. A., Stratiform precipitation in regions of convection: A meteorological paradox, *Bull. Am. Meteorol. Soc.*, *78*, 2179–2196, 1997.

Janowiak, J. E., and P. A. Arkin, Rainfall variations in the tropics during, 1986–1989 as estimated from observations of cloud-top temperature, *J. Geophys. Res.*, *96*, 3359–3373, 1991.

Kato, S., *Dynamics of the Upper Atmosphere*, Cent. for Acad. Publ., Tokyo, 1980.

Kato, S., T. Tsuda, and F. Wantanabe, Thermal excitation of non-migrating tides, *J. Atmos. Terr. Phys.*, *44*, 131–146, 1982.

Khattatov, B. V., et al., Dynamics of the mesosphere and lower thermosphere as seen by MF radars and the High-Resolution Doppler Imager/UARS, *J. Geophys. Res.*, *101*, 10,393–10,404, 1996.

Lieberman, R. S., and C. B. Leovy, A numerical model of nonmigrating diurnal tides between the surface and 65 km, *J. Atmos. Sci.*, *52*, 389–409, 1995.

Lindzen, R. S., Effect of daily variations of cumulonimbus activity on the atmospheric semidiurnal tide, *Mon. Weather Rev.*, *106*, 526–533, 1978.

Mayr, H. G., J. G. Mengel, K. L. Chan, and H. S. Porter, Seasonal variations of the diurnal tide induced by gravity wave filtering, *Geophys. Res. Lett.*, *25*, 943–946, 1998.

McLandress, C., Seasonal variability of the propagating diurnal tide: Results from the Canadian Middle Atmosphere Model, *J. Geophys. Res.*, *102*, 29,747–29,764, 1997.

McLandress, C., On the importance of gravity waves in the middle atmosphere and their parameterization in general circulation models, *J. Atmos. Sol. Terr. Phys.*, *60*, 1357–1383, 1998.

McLandress, C., The seasonal variation of the propagating diurnal tide in the mesosphere and lower thermosphere, part I, The role of gravity waves and planetary waves, *J. Atmos. Sci.*, *59*, 893–906, 2001.

McLandress, C., and W. E. Ward, Tidal/gravity wave interactions and their influence on the large-scale dynamics of the middle atmosphere: Model results, *J. Geophys. Res.*, *99*, 8139–8155, 1994.

McLandress, C., G. G. Shepherd, B. H. Solheim, M. D. Burrage, P. B. Hays, and W. R. Skinner, Combined mesosphere/thermosphere winds using WINDII and HRDI data from the Upper Atmosphere Research Satellite, *J. Geophys. Res.*, *101*, 10,441–10,453, 1996.

Meyer, C. K., Gravity wave interactions with the diurnal propagating tide, *J. Geophys. Res.*, *104*, 4223–4239, 1999.

Miyahara, S., and J. M. Forbes, Interaction between gravity waves and the diurnal tide in the mesosphere and lower thermosphere, *J. Meteorol. Soc. Jpn.*, *69*, 523–531, 1991.

Miyahara, S., and Y. Miyoshi, Migrating and nonmigrating atmospheric tides simulated by a middle atmosphere general circulation model, *Adv. Space Res.*, *20*, 1201–1207, 1997.

Miyahara, S., Y. Toshida, and Y. Miyoshi, Dynamical coupling between the lower and upper atmosphere by tides and gravity waves, *J. Atmos. Terr. Phys.*, *55*, 1039–1053, 1993.

Norton, W. A., and J. Thuburn, Sensitivity of mesospheric mean flow, planetary waves, and tides to strength of gravity wave drag, *J. Geophys. Res.*, *104*, 30,897–30,912, 1999.

Talaat, E. R., and R. S. Lieberman, Nonmigrating diurnal tides in mesospheric and lower-thermospheric winds and temperatures, *J. Atmos. Sci.*, *56*, 4073–4087, 1999.

Tokioka, T., and I. Yagai, Atmospheric tides appearing in a global atmospheric general circulation model, *J. Meteorol. Soc. Jpn.*, *65*, 423–437, 1987.

Tsuda, T., and S. Kato, Diurnal non-migrating tides excited by a differential heating due to land-sea distribution, *J. Meteorol. Soc. Jpn.*, *67*, 43–54, 1989.

Vial, F., Tides in the middle atmosphere, *J. Atmos. Terr. Phys.*, *51*, 3–17, 1989.

Vial, F., and J. M. Forbes, Recent progress in tidal modeling, *J. Atmos. Terr. Phys.*, *51*, 663–671, 1989.

Vincent, R. A., T. Tsuda, and S. Kato, Asymmetries in mesospheric tidal structure, *J. Atmos. Terr. Phys.*, *51*, 609–616, 1989.

Volland, H., *Atmospheric Tidal and Planetary Waves*, Kluwer Acad., Norwell, Mass., 1988.

Williams, C. R., and S. K. Avery, Non-migrating diurnal tides forced by deep convective clouds, *J. Geophys. Res.*, *101*, 4079–4091, 1996.

Yagai, I., Non-migrating thermal tides detected in data analysis and a general circulation model, *J. Geophys. Res.*, *94*, 6341–6356, 1989.

J. M. Forbes, Department of Aerospace Engineering Sciences, Campus Box 429, Boulder, CO 80309, USA. (forbes@zeke.colorado.edu)

M. E. Hagan, High Altitude Observatory, National Center for Atmospheric Research, 3450 Mitchell Lane, Boulder, CO 80301, USA. (hagan@ucar.edu)